Tribology International 120 (2018) 105–114

Contents lists available at ScienceDirect

Tribology International

journal homepage: www.elsevier.com/locate/triboint

A new damage-mechanics-based model for rolling contact fatigue analysis of cylindrical roller bearing

Fukai Li [a], Weiping Hu [a,*], Qingchun Meng [a], Zhixin Zhan [b], Fei Shen [b]

[a] School of Aeronautics Science and Engineering, Beihang University, Beijing 100191, China
[b] School of Mechanical and Aerospace Engineering, Nanyang Technological University, 639798, Singapore

ARTICLE INFO

Keywords:
Rolling contact fatigue
Damage mechanics
Explicit finite element
Crack initiation
Crack propagation

ABSTRACT

The cyclic contact stresses in cylindrical roller bearings are evaluated through the explicit finite element analysis with rolling the roller instead of moving a constant contact pressure in the computational domain. A new damage evolution equation in terms of the amplitude of octahedral shear stress is proposed, which considers the non-proportional variation of stress, and the material parameters in which are easily obtained from torsion fatigue testing data. Numerical simulations of crack initiation, crack propagation, and spalling are performed. The simulation results are consistent with the previous experimental results. Furthermore, the coupling effect between the contact stresses and fatigue damage is investigated, and the effects of contact loading on the fatigue life are studied.

1. Introduction

Roller bearings are widely used in several types of mechanical equipments, especially transmission systems and engines. Since bearing rollers periodically roll between the raceway surfaces of the inner and outer rings, the rings are subjected to cyclic contact stresses, which can lead to the fatigue failure of bearings i.e. rolling contact fatigue (RCF). Generally, the outer ring is more prone to failure in the form of spalling on the contact surface. This is because that the number of contact cycles between the roller and outer ring is more than that between the roller and inner ring because the outer ring is usually fixed. Therefore, the RCF of the outer ring is of significant concern and has received intensive research attention.

RCF differs from the classical fatigue in several aspects, which makes it a challenging issue. First, the cyclic stress that leads to the fatigue failure of the outer ring is induced by the contact between the roller and the raceway surface of the outer ring. Therefore, the critical zone is highly localised and the stress state of the material in this zone is multi-axial. Second, in one loading cycle, the stress components vary non-proportionally owing to the nonlinearity of the contact state. Third, the contact state may keep changing with the evolution of fatigue damage; in other words, the coupling effect between contact analysis and fatigue damage calculation should be considered. These factors result in the complexity of RCF and pose difficulties in gaining an understanding of its mechanism.

In recent decades, experimental studies have extensively been conducted with the aim of observing the characteristics of RCF and understanding its mechanism. Zhao et al. [1] conducted an experimental study of the subsurface crack propagation behaviour of silicon nitride under lubricated rolling contact condition. Their results revealed that the RCF life was mostly influenced by the contact loading and the lubricating fluid. Examination showed that the original ring crack propagated during fatigue testing and crack branching occurred. Furthermore, secondary surface cracks were observed, especially under high contact stress. Forster [2] conducted experiments of the RCF life endurance and spall propagation on 208-size angular-contact ball bearings made of three materials: AISI 52100, AISI M50, and M50Nil. Spall propagation experiments showed that all materials exhibited a rapid or critical spall growth rate after undergoing initial low-rate spall growth. The growth rate was dependent on the contact stress and was considerably fast in AISI 52100 steel. Chen et al. [3] performed continuous observations of the initiation, propagation, and failure of subsurface crack due to rolling contact in GCr15 bearing steel. The mechanical behaviour of each stage was independent and distinct and could be easily separated from each other. They also found that the residual stresses strongly influenced the propagation angle of a subsurface crack in rolling contact. This angle was larger under larger tensile residual stresses and smaller under larger compressive residual stresses.

Since cyclic contact stresses are the primary cause of fatigue failure of rings, the first issue of concern is the analysis of contact stress. Hertz [4]

* Corresponding author. Room D604, New Main Building, 37th Xueyuan Road, Beihang University, Beijing 100191, China.
E-mail address: huweiping@buaa.edu.cn (W. Hu).

https://doi.org/10.1016/j.triboint.2017.12.001
Received 26 September 2017; Received in revised form 1 December 2017; Accepted 2 December 2017
Available online 12 December 2017
0301-679X/© 2017 Elsevier Ltd. All rights reserved.

presented a classical analytical solution of normal contact between two semi-infinite elastic bodies. This solution was widely used in the approximate analysis of engineering structures or adopted for the verification of numerical models. Contact stress analysis of most engineering structures relies only on numerical approaches. Bogdanski et al. [5] presented the results of stress analysis of rail RCF cracks using the finite element (FE) method, which enabled the stress field at the crack tip to be described by the stress intensity factors in the framework of fracture mechanics. Overall, the use of a numerical method is an effective approach for the analysis of rolling contact stress in complex engineering structures. However, the numerical model should first bevalidated by comparison with the Hertzian solution.

Owing to the complexity of contact stress distribution and the nonlinearity of variation of the stress field during periodic rolling contact, it is difficult to establish the correlation between the fatigue life of the rings and the rolling contact stresses. Over the years, many models have been proposed to predict the lives of roller bearings in RCF. These models can be classified as probabilistic and deterministic models [6]. On the one hand, probabilistic models are largely empirical in nature and include variables obtained via extensive experimental testing. Several researchers such as Lundberg and Palmgren [7,8], Tallian [9], and Parker and Zaretsky [10], carefully studied probabilistic models for RCF life. Among these models, the one proposed by Lundberg and Palmgren [7,8], termed the LP model, is considered as the classical model and has been widely used for predicting the RCF life of roller bearings. Although probabilistic models can provide a reasonable prediction of fatigue life, they do not directly consider the details of the constitutive behaviour of materials under contact loading; they also do not involve computations of the residual stress and strain in the contact areas.

Deterministic models, on the other hand, take into account the actual mechanics of the failure process and the constitutive behaviour of materials to predict the RCF lives. Under the assumption that the crack initiation life is negligible in comparison to the crack propagation life, Keer and Bryant [11] utilised the two-dimensional fracture mechanics approach to evaluate fatigue lives in rolling/sliding Hertzian contacts. In their study, a crack was assumed to be embedded in a rolling wheel, and cyclic loading was simulated under the assumption that stresses having a Hertzian distribution travel across the half space. The fatigue life could be predicted by increasing the length of the crack and calculating the stress intensity factor. By assuming that the RCF life is compromised by crack initiation and crack propagation, Zhou et al. [12] proposed a life model that included both the crack initiation life and crack propagation life. They presented a micro-macro contact model for surface pitting in rolling and sliding contacts. In their study, cracking was assumed to occur when the accumulated strain energy of the dislocation reached a critical value, and a three-dimensional crack propagating model was also used for predicting the crack propagation life. Similarly, a micromechanical model based on the dislocation pile-up theory was proposed by Cheng et al. [13] to predict the crack initiation life in RCF. The influences of residual stress, hardness, and temperature on the crack initiation life were discussed.

The above mentioned approaches can be used to predict the RCF life. However, they cannot describe the evolution process of fatigue damage or reflect the coupling effect between the contact stress field and the RCF damage. A continuum damage mechanics (CDM) approach has been proposed to calculate fatigue life, wherein a damage evolution equation was developed to describe the process of fatigue damage [14–16]. A damage-mechanics-based model considers both the crack initiation and crack propagation stages in a unified framework, and facilitates both the evaluation of the crack initiation and crack propagation lives and investigation of the mechanisms of these two stages separately. Damage-mechanics-based approaches have been successfully adopted in the life prediction of many types of fatigue problems, such as fretting fatigue [17,18], defect tolerance analysis [19,20], and bolt fastener fatigue [21–23]. Weinzapfel and Sadeghi [24] and Slack and Sadeghi [25,26] presented a series of CDM-based methods to simulate subsurface crack initiation and propagation in RCF. All these methods [24–26] considered shear stress along grain boundaries as the failure-causing stress in fatigue life prediction and effectively simulated the entire process of subsurface crack initiation and propagation. However, these models have a drawback in that the stress history of materials was obtained by moving a constant distribution of Hertzian pressure over the computational domain. However, in practical applications, the distribution of contact pressure varies with the evolution of fatigue damage.

This study aims to develop a damage-mechanics-based approach for subsurface-originated RCF of the outer ring of a cylindrical roller bearing. First, a two-dimensional explicit FE model is built in ABAQUS to calculate the cyclic rolling contact stresses. In the model, the roller is set to repeatedly roll across the surface of the outer ring. Thus, the variation of contact stresses with an increase in the number of rolling cycles can be accurately considered, thereby making it superior to the method that uses a pre-calculated Hertzian distributed pressure moving along the surface of the outer ring [24–26]. Second, a new damage evolution equation expressed in terms of the amplitude of octahedral shearing stress, which considers the non-proportional variation of stress, is established in order to describe the development of RCF damage. The material parameters included in the equation can be easily determined from torsion fatigue testing data. A numerical simulation of the accumulation of fatigue damage with an increase in the number of rolling cycles is performed using the VUMAT subroutine in ABAQUS. The processes of crack initiation and crack propagation are simulated. Furthermore, the spalling morphology and RCF life are predicted and compared with the previous experimental results. Finally, the coupling effects between the contact stress and fatigue damage are studied in detail and the effects of the contact pressure on fatigue life are investigated.

2. Rolling contact stress analysis

2.1. FE model

A schematic diagram of the contact between the roller and outer ring is shown in Fig. 1. In the figure, R_1 and R_2 are the radii of the roller and outer ring, respectively. P denotes the load borne by the bearing per unit length. In view of the uniformity of loading distribution along the axial direction, the model can be simplified into a line contact (plane strain condition), which typically occurs in roller bearings [24–26]. As shown in Fig. 2, the radius of the rollerR_1, is 9 mm, and the radius of the outer racewayR_2, is 56.5 mm. A reference point (RF) is set at the centre of the roller, and the RF is coupled with the roller. Both the roller and outer ring are made of AISI-52100 steel. The thickness of the outer ring is 17 mm. There are twelve rollers rolling across the ring and hence, the entire ring can be divided into twelve parts of an average length of approximately 30 mm. Considering the application of periodical boundary conditions and stress distribution along the thickness of the outer ring, the calculated part of the outer ring is a rectangle with a height of 15 mm and width of 30 mm. The results indicate that the chosen domain dimensions are reasonable to model the actual contact conditions. The master-slave surface algorithm is employed for simulating the contact between the roller and outer ring. The surface of the roller is set as the master surface,

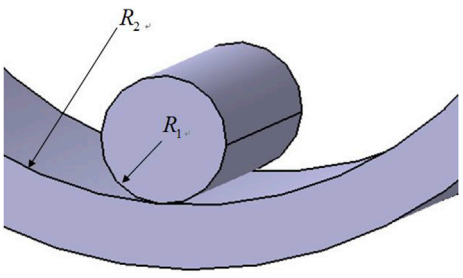

Fig. 1. Schematic diagram of rolling contact between roller and outer ring.

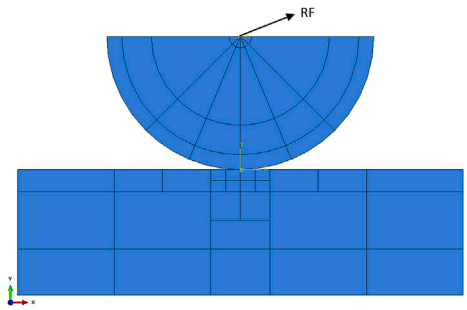

Fig. 2. Geometry of two-dimensional contact model for rolling contact stress analysis.

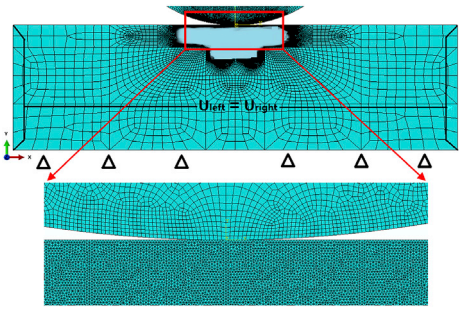

Fig. 3. FE model for rolling contact stress analysis.

and the upper surface of the outer ring is set as the slave surface. The contact type is set as a finite slide, and the kinematic contact method is adopted to simulate the rolling contact. The kinematic contact method is a kind of algorithm provided by ABAQUS [27], and it is usually employed for the case of hard contact with rough friction and no separation relationship. The friction coefficient is set as 0.05 due to the fine lubrication. The plane strain element CPE3 is selected. An element size of 12 μm is used near the contact region; however, away from the contact region the mesh is relatively coarse. This mesh size has been chosen to provide an accurate stress solution and convergent fatigue life value. The parameters of the material and FE model are listed in Table 1. All the displacements at the bottom of the outer ring are fixed, and a periodic boundary condition is applied, in which the displacement of the surface at the left is the same as that of the surface at the right. As shown in Fig. 3, a displacement of 0.012 mm is applied at the RF along the Y-axis to generate the contact load. Many researchers have used the application of constant forces in rolling contact analysis. However, the application of force results in instabilities in the calculation of the explicit solution. Therefore, a constant displacement, rather than a constant force, is applied in this study. For the purpose of obtaining an equivalent model, the maximum contact pressures calculated using the two methods are verified. However, we could only verify the initial contact pressure. It is known that, under the condition of constant displacement, the contact force will decrease, induced by the damage of the ring. The calculation result shows that the decrease is not significant and mainly occurs at the end stage of fatigue. Therefore, the constant displacement method is slightly more conservative than the constant force method.

An explicit FE model is adopted in this research; it offers the following two advantages over an implicit FE model in the context of the present study. First, the use of an explicit FE model facilitates a much smaller interval, which provides a more complete history of the subsurface stresses without increasing the computational cost. Second, the explicit FE model can maintain the stability of calculation even when the elastic moduli of some elements degenerate significantly.

It is worth noting that the quasi-static contact condition should be satisfied when using the explicit method. The quasi static condition is satisfied by setting a limit on the ratio of kinetic energy and internal energy in ABAQUS. Several parameters, such as the linear bulk viscosity, quadratic bulk viscosity, and mass scaling coefficient, may be adjusted to obtain a reasonable value of the ratio. Usually, when the value of the ratio is lower than 5%–10%, the quasi static condition is considered satisfied. The ratio is kept lower than 10% in the present model.

For the purpose of validating the developed FE model, a static contact stress analysis is performed to compare its results with those of the theoretical Hertz solution. Fig. 4(a)–(c) compare the results from the FE model for the contact pressure and stress components σ_{xx} and σ_{yy} under the static contact condition with those of the Hertz theoretical solution. The comparison reveals that the FE model can accurately simulate the static contact between the roller and outer ring. This model is further used for the rolling contact stress analysis, which is detailed in Section 2.2.

It can be observed that the calculated maximum contact pressure in the static contact stress analysis is slightly lower than the given value of 2.5 GPa. This is attributed to that the displacement loading determined by the consistence condition of maximum contact pressure in the rolling contact analysis is directly applied in the static contact analysis. The maximum contact pressure in the rolling contact stress analysis can reach approximately 2.5 GPa due to the slight dynamic effect in the explicit solution.

2.2. Rolling contact stress analysis

The rolling contact condition considered in this study is pure rolling. Loading is applied in two steps:

(1) The roller is placed at the centre of the upper surface of the outer ring and a displacement is applied along the Y-direction at the RF to generate a contact load.
(2) A translational displacement with an amplitude of 0.45 mm and a rotary displacement with an amplitude of 0.05 rad are applied at the RF, as shown in Fig. 5. The roller periodically rolls back and forth over the domain in a 8-s cycle. It should be noted that in practice, the roller rolls in a single direction rather than back and forth. However, it is inconvenient to simulate the contact with a single rolling direction. Thus, we allow the roller to move back and forth; however, the rolling contact stress analysis is performed only when the roller rolls forward. That is, the backward motion of the roller only enables it to return to the initial position.

Fig. 6 illustrates the variation of stress components at a point on the contact surface in one loading cycle. Fig. 7 illustrates the variation of stress components at a point located at the depth with the maximum σ_{xy} in one loading cycle. Figs. 6 and 7 reveal that the stress components are non-proportional, irrespective of whether they are on the contact surface or subsurface. This characteristic of non-proportional variation must be considered in the calculation of damage driving force.

Table 1
Parameters of material and FE model.

Elastic modulus (GPa)	Poisson's ratio	Density (kg/m^3)	Maximum contact pressure (MPa)	Roller translational velocity (μm/s)	Mass scaling coefficient	Surface friction coefficient
200	0.3	7800	2500	225	2×10^8	0.05

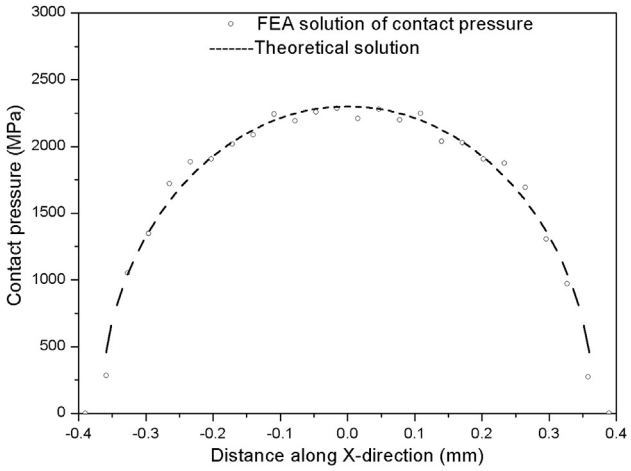

(a)

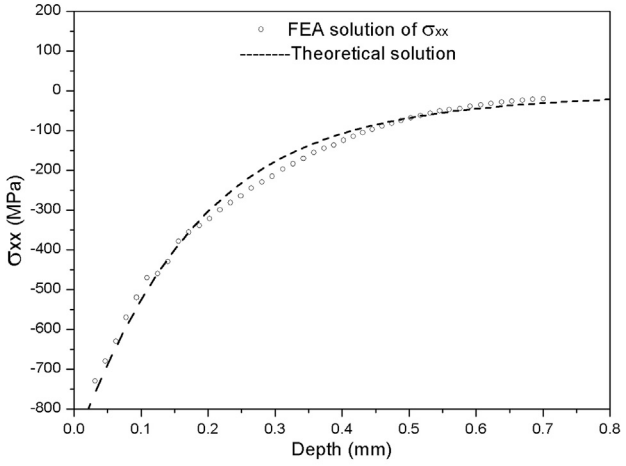

(b)

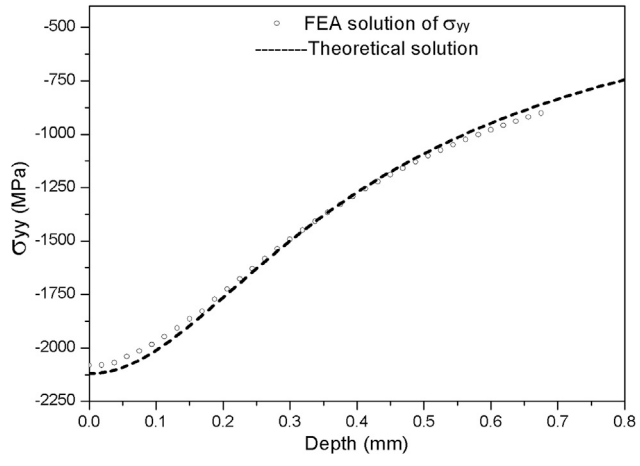

(c)

Fig. 4. Comparison between the simulation and theoretical results of (a) contact pressure; (b) stress along X-direction, σ_{xx}; (c)stress along Y-direction, σ_{yy}.

3. Fatigue damage model

3.1. Damage variables

Damage refers to the formation and growth of micro-cracks or micro-voids, which are discontinuities in a medium considered continuous at a large scale [28]. In engineering, the mechanics of continuous media can be described by a representative volume element (RVE). In CDM theory, damage of a material is expressed as the stiffness reduction of RVE. Under

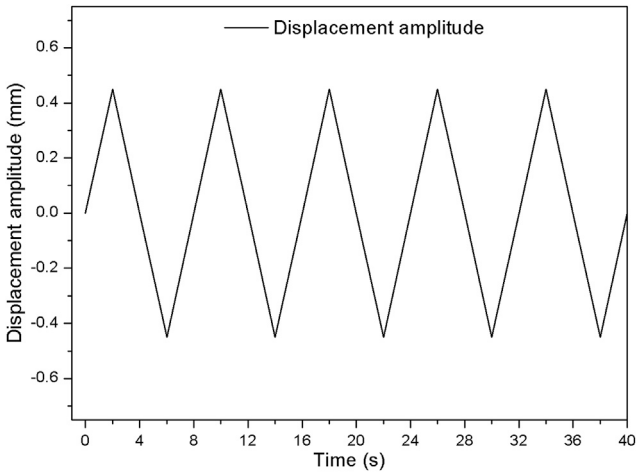

Fig. 5. Displacement of the roller along X-direction.

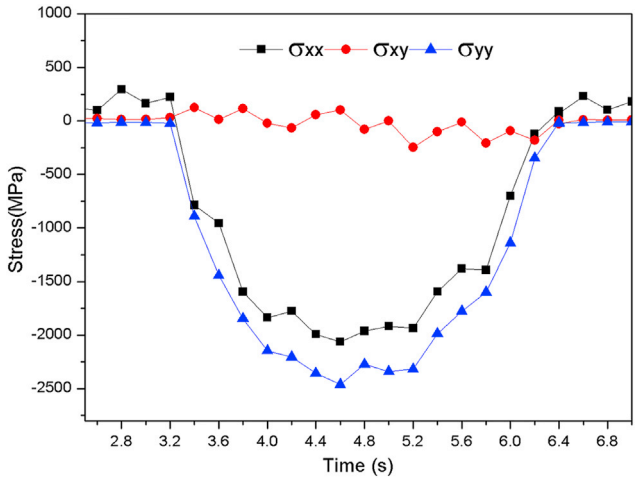

Fig. 6. Variation of stress components at a point on the contact surface in one loading cycle.

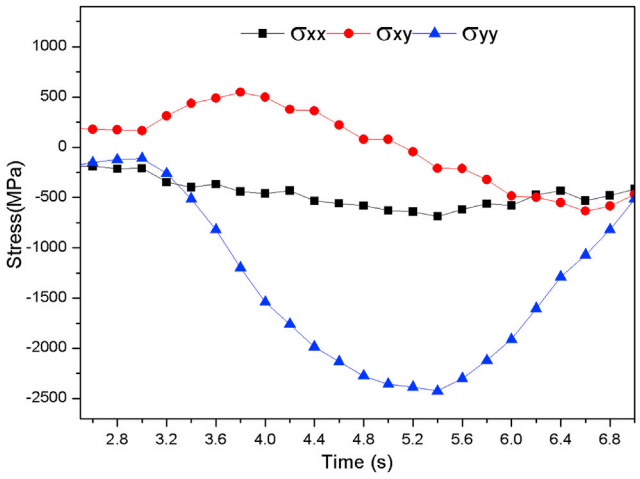

Fig. 7. Variation of stress components at a point located at the depth with the maximum σ_{xy} in one loading cycle.

the assumption of isotropic damage, the scalar damage variable D is defined as

$$D = \frac{E - E_D}{E} \tag{1}$$

where E and E_D are the elastic moduli of RVE without and with damage, respectively.

Damage accumulates in the material with an increase in the number of loading cycles. Macro-cracks initiate when the damage reaches a critical value. From the CDM theory, a damage of 0 indicates that the material is perfect and 1 represents the complete failure of the material. Therefore, the theoretical critical value is 1. In practice, the damage of material is usually less than 1, which is reached immediately before failure during the test. This critical value of damage should be determined by the test. However, it is difficult to obtain this value using a fatigue test. Therefore, the critical value is considered as 1 for crack initiation analysis in high-cycle fatigue [29] for the purpose of simplicity. However, when the crack propagation is involved, the critical value cannot be considered as 1 to ensure the stability of calculation. In the present study, we select a value of 0.95, which can ensure a stable numerical calculation but is slightly less than the critical value of 1. Furthermore, it is known that a major part of fatigue life is consumed at the early stage of damage. Accordingly, this critical value is acceptable to model the real condition approximately.

3.2. Damage-coupled constitutive equation

According to the hypothesis of strain equivalence, the damage-coupled constitutive equation for the case of elastic deformation is derived as follows [30]:

$$\sigma_{ij} = C^E_{ijkl}(1 - D)\varepsilon^E_{kl} \tag{2}$$

where σ_{ij} is the Cauchy stress, C^E_{ijkl} is the material stiffness, and ε^E_{kl} is the strain.

3.3. Damage evolution equation

Harris and Yu [31] determined that the subsurface octahedral shear stress distribution could reflect the effects of surface shear stresses on fatigue lives. Furthermore, the octahedral stress was adopted in the damage model of Chaboche [32], and this model has been used effectively for high cycle fatigue problems. Therefore, it is reasonable to consider the octahedral shear stress as the failure-causing stress in fatigue life prediction. Weinzapfel and Sadeghi [24] and Slack and Sadeghi [25, 26] presented a series of damage evolution equations that considered the range of shear stresses acting on a particular grain boundary. On the basis of the failure-causing stress in Ref. [31] and the form of the damage evolution equation in Refs. [24–26], we propose a new damage evolution equation herein:

$$\frac{dD}{dN} = \left[\frac{\Delta\tau_8}{\tau_r(1 - D)}\right]^m \tag{3}$$

where τ_r and m are material parameters, which can be determined from the experimental data, and $\Delta\tau_8$ is the octahedral shear stress amplitude. In consideration of the non-proportional variation of the contact stress components, the expression for the calculation of $\Delta\tau_8$ is given as

$$\Delta\tau_8 = \frac{1}{2}\max_{t}\max_{t_0}\left[\frac{3}{2}\left(s_{ij,t} - s_{ij,t_0}\right)\left(s_{ij,t} - s_{ij,t_0}\right)\right]^{1/2} \tag{4}$$

where $s_{ij,t}$ and s_{ij,t_0} denote components of the deviatoric stress tensor ij at different times within a loading cycle. Notably, the amplitude of octahedral stress is not the difference between the highest and lowest stresses in one cycle for the rolling contact case. As the stress state varies non-proportionally, it is difficult to define the highest and lowest stresses. Accordingly, each cycle is divided into many intervals, and t_0 and t represent two arbitrary time points during a cycle. Based on the stresses at the two given time points, a candidate of the octahedral shear stress amplitude is calculated. $\Delta\tau_8$ is obtained by determining the maximum value among these candidates at different time points.

3.4. Determination of material parameters

As mentioned before, two parameters τ_r and m are included in the damage evolution equation (Eq. (3)). These two parameters are assumed to be material parameters independent of the stress state for fatigue failure induced mainly by shearing stresses. Accordingly, the data of torsion fatigue test are used for the determination of the two parameters.

First, under the stress control test condition, the shearing stress range was assumed to be constant. Further, we neglected the difference between the critical values of 0.95 and 1. Thus, a simple integration of Eq. (3) can be expressed as

$$\begin{aligned}\int_0^{N_f} dN &= \int_0^{0.95}\left\{\frac{\tau_r(1 - D)}{\Delta\tau_8}\right\}^m dD \approx \int_0^1\left\{\frac{\tau_r(1 - D)}{\Delta\tau_8}\right\}^m dD \\ &= \left(\frac{\tau_r}{\Delta\tau_8}\right)^m \int_0^1 (1 - D)^m dD\end{aligned} \tag{5}$$

Finally, we have

$$N_f = \frac{1}{m + 1}\left[\frac{\tau_r}{\Delta\tau_8}\right]^m \tag{6}$$

where N_f is the number of cycles to failure. The conventional stress–life curve for a torsion fatigue test is given by Ref. [33].

$$\frac{\Delta\tau}{2} = \tau_{f1}\left(N_f\right)^{1/B_1} \tag{7}$$

where $\Delta\tau$ is the orthogonal shear stress amplitude, and B_1 and τ_{f1} are the slope and stress-axis intercept, respectively, of the $\Delta\tau - N$ curve for the material in torsion fatigue, as shown in Fig. 8. Eq. (7) can be expressed in terms of $\Delta\tau_8$ as follows:

$$\frac{\Delta\tau_8}{2} = \tau_f\left(N_f\right)^{1/B} \tag{8}$$

where B and τ_f are the slope and stress-axis intercept, respectively, of the $\Delta\tau_8 - N$ curve for the material in torsion fatigue.

Subsequently, by integrating Eq. (8), we can obtain the expression of fatigue life:

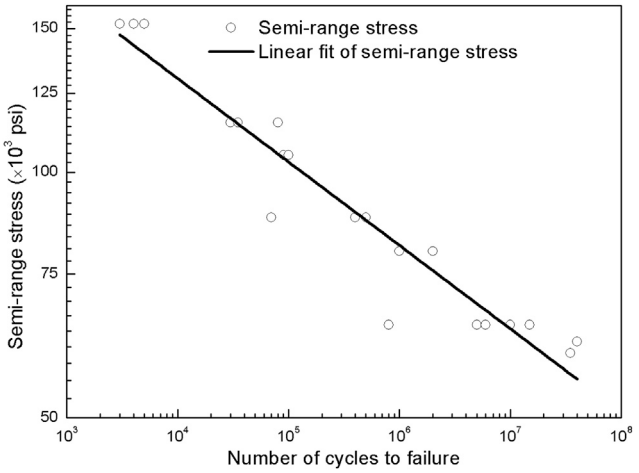

Fig. 8. S–N curve for AISI-52100 bearing steel in completely reversed torsion [33].

$$N_f = \left[\frac{2\tau_f}{\Delta\tau_8}\right]^B \tag{9}$$

Comparing Eq. (6) with (9) gives

$$\frac{1}{m+1}\left[\frac{\tau_r}{\Delta\tau_8}\right]^m = \left[\frac{2\tau_f}{\Delta\tau_8}\right]^B \tag{10}$$

Thus, the following can be derived:

$$m = B, \tau_r = 2\tau_f(B+1)^{1/B} \tag{11}$$

Fig. 8 shows the experimentally obtained $\Delta\tau - N$ curve and the fitted curve for the AISI-52100 bearing steel [33]. Subsequently, the values of the two material parameters can be easily determined as follows:

$$m = 10.1, \tau_r = 4991 \text{ MPa} \tag{12}$$

4. Numerical algorithm for accumulation of fatigue damage

Generally, the process of fatigue failure of the outer ring can be considered to occur in two stages: crack initiation and crack propagation. In the following section, we present, in detail, a numerical algorithm for the accumulation of fatigue damage in these two stages.

4.1. Numerical algorithm for crack initiation

Crack initiation analysis involves the calculation of the rolling contact stress, computation of damage progress, and recalculation of stiffness degradation and rolling stress until the criterion for crack initiation, which is defined as $D = 0.95$, is satisfied. On the basis of the stress analysis method and theoretical damage model presented in Section 2 and Section 3, a numerical algorithm is developed for describing the crack initiation process using decoupling of the damage evolution calculation and stress analysis. Since it is computationally expensive to simulate each loading cycle, a jump-in-cycles procedure [28] is adopted in the numerical implementation, which assumes that the contact stresses and damage progress are the same in each cycle in a block containing ΔN cycles. Thus, the damage evolution can be interpreted to be piecewise linear with respect to the number of cycles. Notably, the value of ΔN is determined to obtain a convergent fatigue life. The detailed calculation steps are as follows:

(1) Before the start of simulation, the entire material is assumed to be undamaged, and hence, the initial damage to each element is assumed to be 0.

$$D_j^0 = 0 \tag{13}$$

where j is the element number. In fact, the damage D is defined at the integration point of each element. However, the element type CPE3 taken in the current model is a type of constant strain element with only one integration point. Therefore, the damage at the integration point is the same as that of the element.

(2) The octahedral shear stress amplitude $(\Delta\tau_8)_j^i$ for the current block i is calculated using the rolling contact stress analysis method presented in Section 2.

(3) According to the analysis result of rolling contact stresses in one cycle, the damage evolution rate for each element in the rolling contact domain is calculated using the damage evolution equation (Eq. (3)):

$$\left(\frac{dD}{dN}\right)_j^i = \left[\frac{(\Delta\tau_8)_j^i}{\tau_r\left(1 - D_j^i\right)}\right]^m \tag{14}$$

(4) The damage and elastic modulus of each element at the end of block i are updated as follows:

$$D_j^{i+1} = D_j^i + \left(\frac{dD}{dN}\right)_j^i \Delta N \tag{15}$$

$$E_j^{i+1} = E_j^i\left[1 - D_j^{i+1}\right] \tag{16}$$

Generally, according to the literature [34], the value of ΔN is valid when it satisfies the condition $\Delta N/N \leq 0.01 - 0.02$. Furthermore, the value of ΔN varies from one loading case to another. For example, ΔN is 2.0×10^4 for the initial maximum contact pressure of 2.5 GPa and 1.4×10^6 for the contact pressure of 1.5 GPa.

(5) The algorithm repeats steps (2)–(4) for each block until the accumulated damage at any integration point reaches the critical value $D_c = 0.95$. The corresponding number of cycles is defined as the crack initiation life. The stiffness of the elements whose damage reaches the critical value is retained in the global stiffness matrix, rather than being removed for the purpose of stability of calculation.

$$N^{i+1} = N^i + \Delta N \tag{17}$$

The flowchart of the numerical algorithm outlined below is shown in Fig. 9.

4.2. Numerical algorithm for crack propagation

The numerical algorithm for crack propagation involves the following steps.

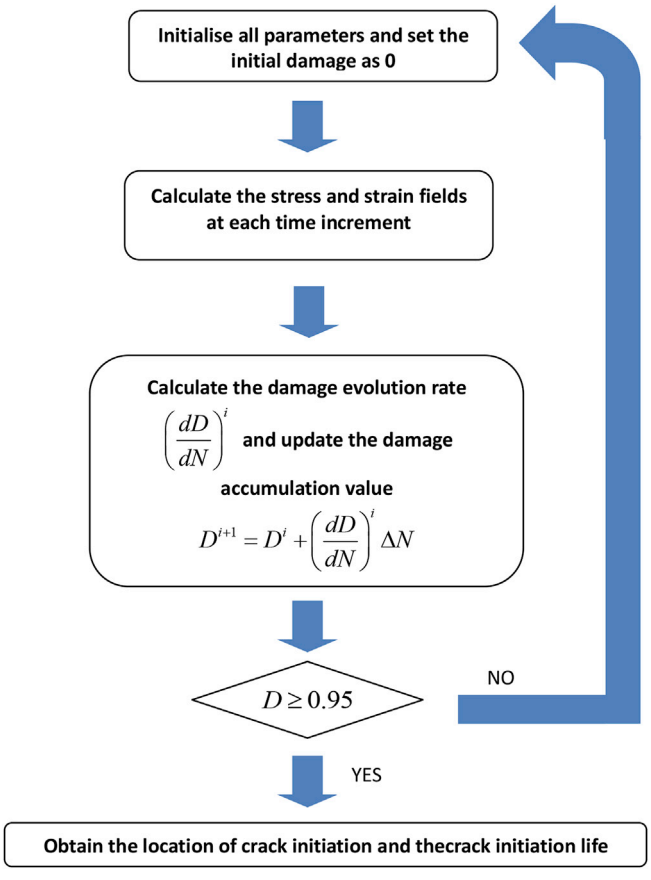

Fig. 9. Flowchart of numerical algorithm for crack initiation.

(1) After the crack initiates, the damage evolution equation, i.e. Eq. (3), is applied to the same FE model in consideration of the present damage field. The damage of the first failure element remains constant at D_c.
(2) The roller continues to roll over the outer-ring surface and the damage evolves continuously in all the elements except the failure element. With an increase in the number of rolling cycles, the damage of the next element reaches the critical value D_c. Subsequently, the second element fails.
(3) Rolling continues, and consequently, an increasing number of elements fail. All of them form a path, which is considered as the crack propagation path. The number of cycles from the failure of the first element to the occurrence of surface spalling is considered as the crack propagation life. The sum of the crack initiation life and crack propagation life is considered as the total fatigue life.

5. Results and discussion

5.1. Comparison of numerical results with experimental results

The simulation results of RCF are compared with the experimental results reported in the literature [2,35,36]. All the experiments were conducted under the same conditions of the material and loading as those adopted in the current FE model. Comparisons of the spall shape and crack propagation length can be found in Ref. [2]. The crack initiation depth was investigated in Ref. [35], and the total fatigue life was evaluated in Ref. [36].

Fig. 10 shows the development of the damage zone with an increase in the number of rolling contact cycles. It can be observed that the first element whose damage reaches D_c is located at the subsurface, which is in the region of maximum octahedral shear stress amplitude. Subsequently, an increasing number of elements near the crack initiation location undergo damage and these damaged elements form the crack. The crack path is observed to be primarily parallel to the surface. With further cyclic rolling, these damaged zones become increasingly longer, subsequently curve towards the contact surface, and eventually reach the surface, thereby forming a semi-elliptical spall; this is consistent with the experimental observations [2] shown in Fig. 11. The crack propagation length obtained from Fig. 11 is approximately 1–2 mm. The crack propagation length in the current FE model is 0.75 mm, which is slightly shorter than the experimental result. The reason for this discrepancy is that the experimental spall may have been caused by the linking of more than one crack band, but only one crack band can be included in the current model. The distributions of $\Delta\tau_8$ in the computational domain at four different times are shown in Fig. 12. From the distributions of $\Delta\tau_8$ before crack initiation and at the instance of crack initiation shown in Fig. 12(a) and (b), respectively, we can observe that the crack initiates at the location where $\Delta\tau_8$ is maximum. Fig. 12(c) shows the distribution of $\Delta\tau_8$ when the crack propagation path starts to curve, which indicates that $\Delta\tau_8$ causes a change in the crack propagation direction. Fig. 12(d) shows the distribution of $\Delta\tau_8$ when the crack propagates to the surface and spalling occurs. It can be observed that, although the values of $\Delta\tau_8$in the damage zone decrease owing to the degeneration of stiffness, the distribution of the maximum $\Delta\tau_8$ is always consistent with the crack propagation path.

In order to study the depth of the location of crack initiation, Chen et al. [35] investigated the subsurface crack initiation depth using experimental observations. In their study, a ring-type rolling fatigue rig made of AISI-521000 steel was tested for the contact pressure of 2450 MPa, and the test results revealed that the depth at which the crack initiated ranged from 0.173 mm to 0.612 mm, and that the average depth was 0.347 mm. The crack initiation depth calculated using the current

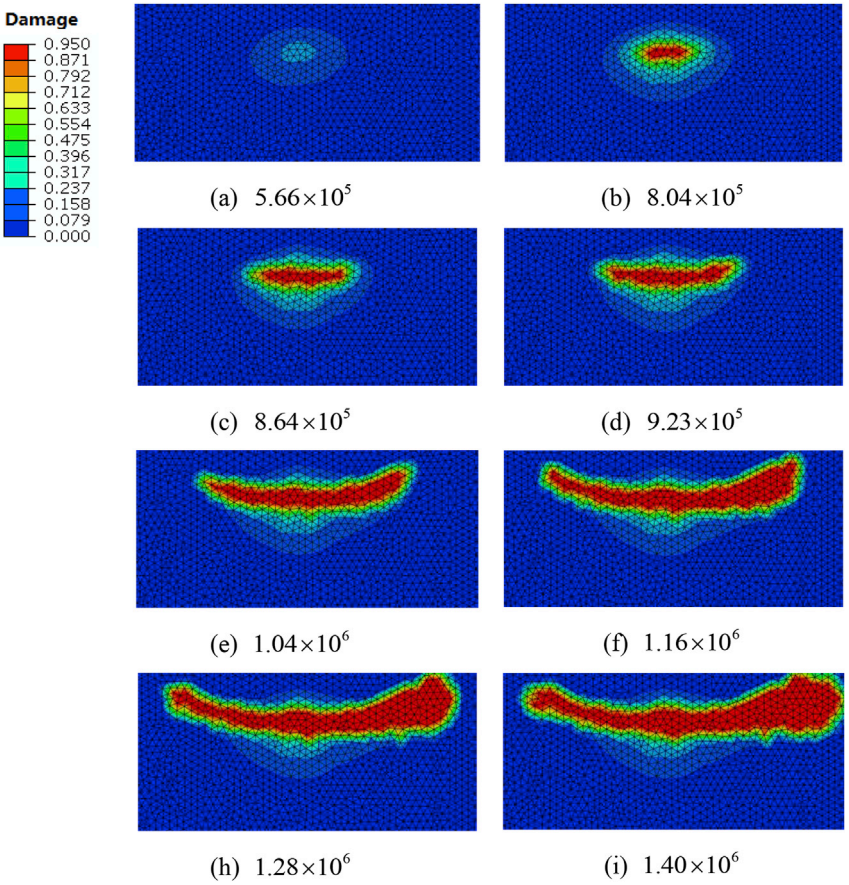

Fig. 10. Formation of subsurface spalling.

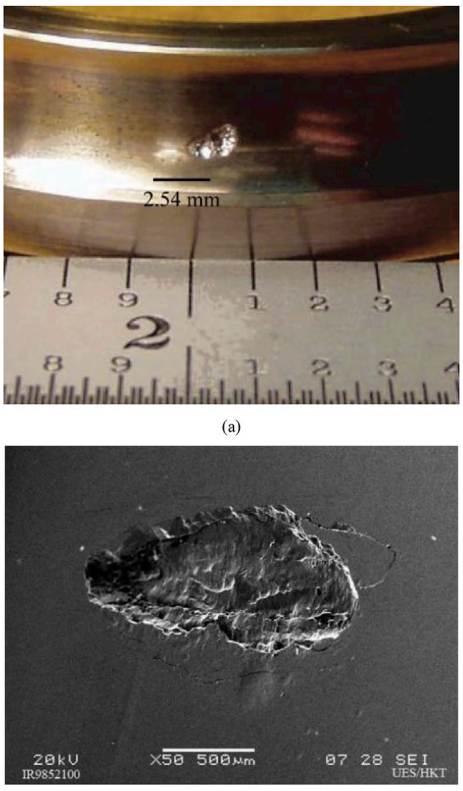

(a)

(b)

Fig. 11. Typical fatigue spall formed on AISI-52100 in endurance life experiments [2].

model under the same condition is 0.23 mm, which lies within the acceptable range of the experimental data.

Qualitatively, the location of crack initiation is directly related to the octahedral stress or von Mises stress. However, the crack does not initiate at the location of the maximum von Mises stress. Moreover, the two locations differ slightly from each other. Accordingly, it is acceptable to approximately predict the depth of crack initiation according to the distribution of von Mises stress. Subsequently, we compare the total fatigue life calculated using the current model with the experimentally determined values in Ref. [36], which were 1.5×10^6, 1.08×10^7, 1.66×10^7, and 1.02×10^8. Under the same conditions, the total RCF life calculated using the current model is 1.4×10^6, which is slightly smaller than the experimental result because the method adopted is conservative. This result is reasonable in view of the wide distribution of fatigue lives in RCF.

5.2. Coupling between contact stresses and fatigue damage

In contrast to the models of Weinzapfel and Sadeghi [24] and Slack and Sadeghi [25,26], in the current model, it is possible to consider the coupling effect between contact pressure and fatigue damage. Paulson et al. [37] and Bomidi et al. [38] investigated the effect of damage on the contact pressure distribution. In the study by Paulson et al., this effect was investigated by reevaluating the elasto-hydrodynamic lubrication (EHL) pressure. Meanwhile, Bomidi et al. adopted a rigid roller model to present the variation of contact pressure distribution. In our study, this coupling effect is investigated through calculating the contact pressure between two elastic bodies during the fatigue process.

Fig. 13 shows the variation of the maximum contact pressure and the evolution of damage at the crack initiation point with an increase in the number of rolling cycles. With an increase in the number of rolling cycles from 0 to 7.5×10^5, the damage increases gradually from 0 to 0.2 and the maximum contact pressure decreases from 2.5 GPa to 1.5 GPa. This phenomenon is attributed to the deterioration of the material owing to the accumulation of fatigue damage.

Fig. 14 illustrates the evolution of the distribution of contact pressure. It can be observed that the value of the maximum contact pressure in the same zone becomes increasingly smaller as the number of rolling cycles increases, whereas both the location of the maximum contact pressure and the distribution shape vary. With an increase in the number of rolling cycles from 0 to 1.19×10^6, the distribution of contact pressure essentially acquires a symmetric parabolic shape; however, it becomes unsymmetrical when the number of rolling cycles exceeds 1.19×10^6. This phenomenon is attributed to the evolution of deterioration of the material in the form of crack initiation and propagation with an increase in the number of rolling cycles.

Fig. 15 illustrates the evolution of the distribution of the stress component σ_{yy} along the rolling direction on the layer at the depth where maximum σ_{xy} occurs. The absolute maximum value of σ_{yy} in the same zone becomes increasingly smaller with an increase in the number of rolling cycles and the location of maximum σ_{yy} also changes. Before crack initiation, the shape of the distribution of σ_{yy} remains almost constant. However, in the crack propagation stage, the distribution of σ_{yy} changes significantly, which reflects the remarkable influence of crack propagation.

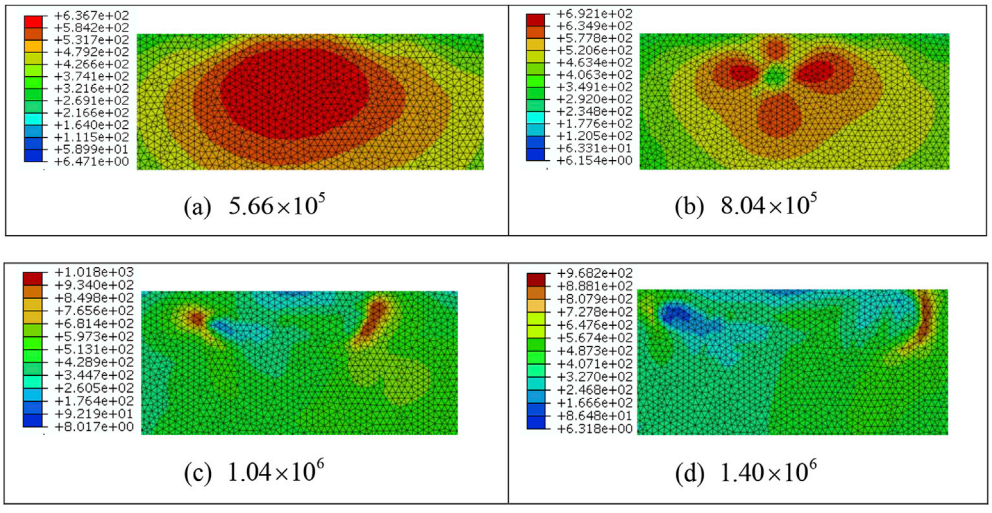

Fig. 12. Distribution of $\Delta\tau_8$ at (a) 5.66×10^5cycles, (b) 8.04×10^5cycles, (c) 1.04×10^6cycles, and (d) 1.40×10^6 cycles.

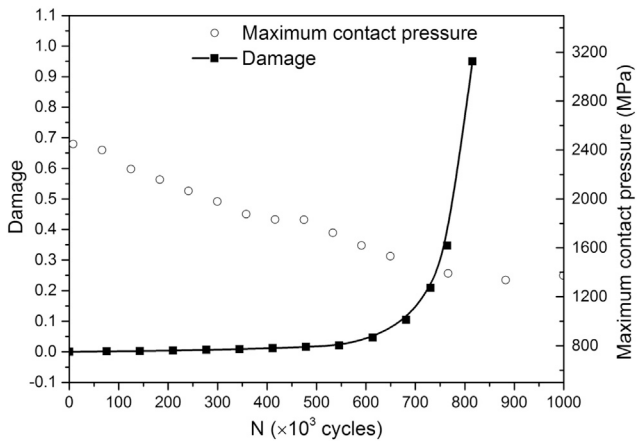

Fig. 13. Evolution of damage at crack initiation point and variation of maximum contact pressure with the number of rolling cycles.

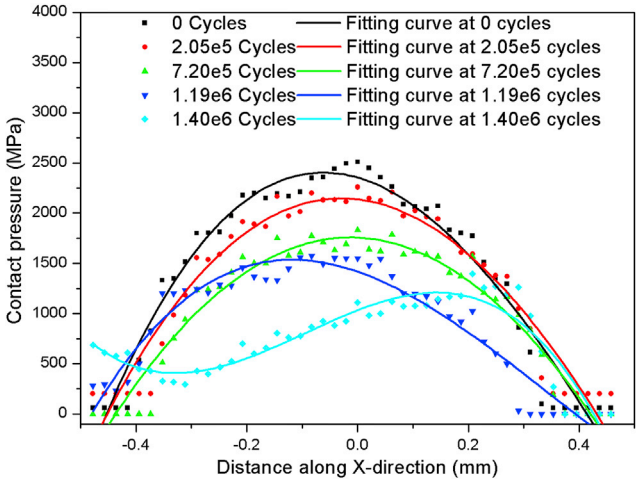

Fig. 14. Evolution of the distribution of contact pressure.

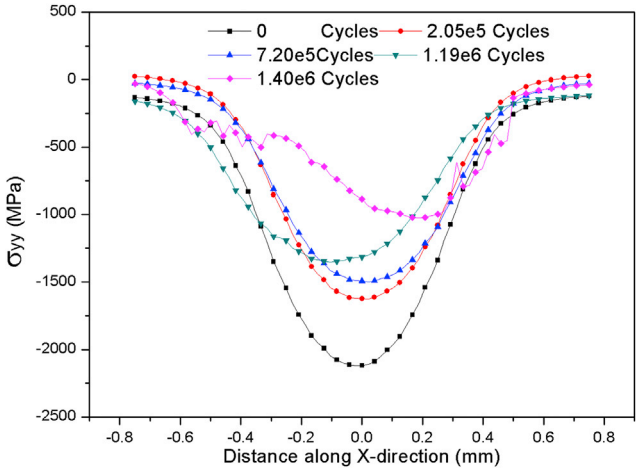

Fig. 15. Evolution of the distribution of stress component σ_{yy} at the depth with maximum σ_{xy}.

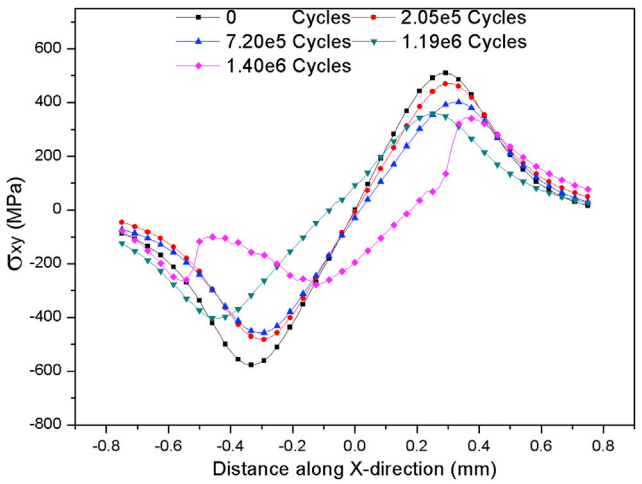

Fig. 16. Evolution of the distribution of stress component σ_{xy} at the depth with maximum σ_{xy}.

Table 2
Crack initiation and total fatigue lives for different initial maximum contact pressures.

P_{max}(GPa)	Crack initiation life	Total fatigue life
1.0	1.47×10^{10}	1.70×10^{10}
1.5	7.06×10^{7}	8.14×10^{7}
1.75	2.56×10^{7}	2.96×10^{7}
2.0	5.35×10^{6}	6.17×10^{6}
2.25	2.05×10^{6}	2.37×10^{6}
2.5	1.19×10^{6}	1.40×10^{6}

Fig. 16 illustrates the evolution of the distribution of the stress component σ_{xy} along the rolling direction on the layer at the depth with maximum σ_{xy}. The inspection of this figure reveals that the effect of fatigue damage on the distribution of this stress component is similar to that observed in Fig. 15.

5.3. *Effects of initial contact pressure on fatigue life*

In order to investigate the effects of the initial contact pressure on the RCF life, several contact loads with initial maximum pressures (P_{max}) ranging from 1 to 2.5 GPa are applied in the calculation. Table 2 lists the crack initiation lives and total fatigue lives calculated using the proposed method for different contact loads. It can be observed that both crack

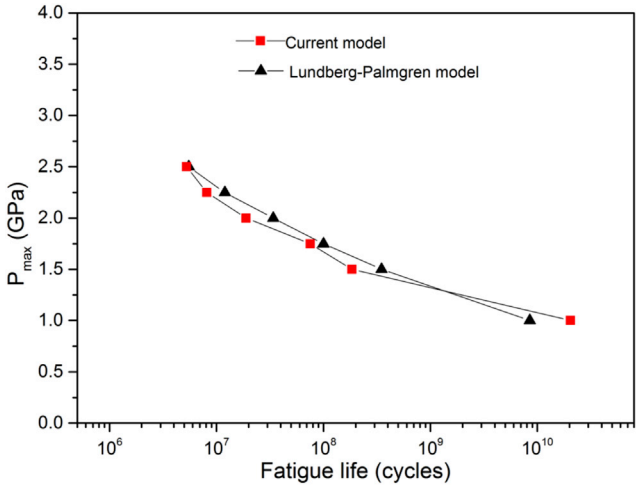

Fig. 17. Comparison between P_{max} vs. fatigue life curves of the current model and LP model (i.e. the theoretical result) for AISI 52100 bearing steel.

initiation life and total fatigue life decrease with an increase in the contact load. Fig. 17 shows a comparison between P_{max} versus fatigue life curves of the current model and the well-known LP model (i.e. the theoretical result) [7,8]. The comparison reveals consistency between the results of the two models.

6. Conclusion

This study proposed a new damage-mechanics-based approach to investigate the crack initiation and propagation in RCF.

First, an explicit FE model is developed for cyclic rolling contact stress analysis, in which the roller rolls along the contact surface. This model reflects the variation of contact loading with the evolution of fatigue damage well.

Second, a new damage evolution equation expressed in terms of the amplitude of octahedral shear stress is established. The non-proportional variation of the stress components in the rolling contact is also considered in this equation. The material parameters in the equation are easily determined from torsion fatigue testing data. Subsequently, a numerical simulation is performed using the VUMAT subroutine in ABAQUS to calculate the accumulation of fatigue damage in the material.

The entire process from the crack initiation to the crack propagation and spalling is simulated. The predicted shape of spall is consistent with the previous experimental observations. Both the predicted depth of the spall and the predicted fatigue life are within the range of the experimental results.

The coupling effects between the contact stresses and fatigue damage are investigated in detail, and the results reveal that fatigue damage before the crack initiation mainly affects the magnitude of the contact stresses and not the shape of their distribution. However, the damage in the crack propagation stage considerably influences both the magnitude of the contact stresses and the shape of their distribution. In addition, the effects of contact pressure on the fatigue life are evaluated, and the results obtained by the developed model are observed to be consistent with those of the well-known LP model.

References

[1] Zhao P, Hadfiel M, Wanga Y, et al. Subsurface propagation of partial ring cracks under rolling contact Part I. Experimental studies. Wear 2006;261(3):382–9.
[2] Forster NH. Rolling contact fatigue life and spall propagation of AISIM50, M50NiL, and AISI 52100, Part I: experimental results. Tribol Trans 2009;53(1):29–41.
[3] Chen L, Chen Q, Shao E. Study on initiation and propagation angles of subsurface cracks in GCr15 bearing steel under rolling contact. Wear 1989;133(2):205–18.
[4] Hertz H. On the contact of rigid elastic solids. Mathematik 1982;92:156–71.
[5] Bogdanski S, Olzak M, Stupnicki J. Numerical stress analysis of rail rolling contact fatigue cracks. Wear 1996;191(1):14–24.
[6] Jalalahmadi B, Slack TS, Raje N, et al. A review of rolling contact fatigue. J Tribol 2009;131(4), 041403. 1-15.
[7] Lungberg G, Pamgren A. Dynamic capacity of rolling bearings. Acta Poly-technica. Ser. Mech. Eng. 1947;1(3):1–50.
[8] Lungberg G, Pamgren A. Dynamic capacity of rolling bearings. Acta Poly-technica. Ser. Mech. Eng. 1952;2(4):1–32.
[9] Tallian Tibor. Weibull distribution of rolling contact fatigue life and deviations therefrom. Tribol Trans 1962;5(1):183–96.
[10] Parker RJ, Zaretsky EV. Rolling-element fatigue life of AISI M-50 and 18-4-1 balls. 1978.
[11] Keer LM, Bryant MD. A pitting model for rolling contact fatigue. J Tribol 1983; 105(2):198–205.
[12] Zhou RS, Cheng HS, Mura T. Micropitting in rolling and sliding contact under mixed lubrication. J Tribol 1989;111(4):605–13.
[13] Cheng W, Cheng HS, Mura T, et al. Micromechanics modeling of crack initiation under contact fatigue. J Tribol 1994;116(1):2–8.
[14] Kachanov LM. Introduction to continuum damage mechanics. M. Nijhoff. 1986.
[15] Chaboche JL. Continuous damage mechanics — a tool to describe phenomena before crack initiation. Nucl Eng Des 1981;64(2):233–47.
[16] Lemaitre J. Mechanics of solid materials. Cambridge: Cambridge Press; 1990.
[17] Shen F, Hu W, Meng Q. A damage mechanics approach to fretting fatigue life prediction with consideration of elastic–plastic damage model and wear. Tribol Int 2015;82:176–90.
[18] Shen F, Hu W, Voyiadjis GZ, et al. Effects of fatigue damage and wear on fretting fatigue under partial slip condition. Wear 2015;s 338–339:394–405.
[19] Zhan Z, Hu W, Zhang M, et al. The fatigue life prediction for structure with surface scratch considering cutting residual stress, initial plasticity damage and fatigue damage. Int J Fatig 2015;74:173–82.
[20] Zhan Z, Hu W, Shen F, et al. Fatigue life calculation for a specimen with an impact pit considering impact damage, residual stress relaxation and elastic-plastic fatigue damage. Int J Fatig 2016;96:208–23.
[21] Sun Y, Voyiadjis GZ, Hu W, et al. Fatigue damage analysis of double-lap bolted joints considering the effects of hole cold expansion and bolt clamping force. J Eng Mater Technol 2017;139(2), 021007. 1-10.
[22] Sun Y, Hu W, Shen F, et al. Numerical simulations of the fatigue damage evolution at a fastener hole treated by cold expansion or with interference fit pin. Int J Mech Sci 2016;107:188–200.
[23] Zhan Z, Meng Q, Hu W, et al. Continuum damage mechanics based approach to study the effects of the scarf angle, surface friction and clamping force over the fatigue life of scarf bolted joints. Int J Fatig 2017;102:59–78.
[24] Weinzapfel N, Sadeghi F. Numerical modeling of sub-surface initiated spalling in rolling contacts. Tribol Int 2013;59(59):210–21.
[25] Slack T, Sadeghi F. Cohesive zone modeling of intergranular fatigue damage in rolling contacts. Tribol Int 2011;44(7):797–804.
[26] Slack T, Sadeghi F. Explicit finite element modeling of subsurface initiated spalling in rolling contacts. Tribol Int 2010;43(9):1693–702.
[27] ABAQUS/Standard version 6.14. Analysis User's guide, vol5. Rhode Island, USA: HibbitKarlsson and Sorensen Inc; 2014.
[28] Lemaitre J, Rodrigue D. Engineering damage mechanics. Springer; 2005.
[29] Murakami S. Continuum damage mechanics : a continuum mechanics approach to the analysis of damage and fracture, vol. 41. Springer Ebooks; 2012. p. 4731–55 (B4).
[30] Lemaitre JA. Course on damage mechanics. Berlin: Springer-Verlag; 1992.
[31] Harris TA, Yu WK. Lundberg-palmgren fatigue theory: considerations of failure stress and stressed volume. J Tribol 1999;121(1):85–9.
[32] Chaboche JL, Lesne PM. A non-linear continuous fatigue damage model. Fatig Fract Eng Mater Struct 1988;11(1):1–17.
[33] Styri H. Fatigue strength of ball bearing races and heat-treated 52100 steel specimens. Proc. Am. Soc. for Test. Mater 1951;51:682–700.
[34] Zhang T, Mchugh PE, Leen SB. Finite element implementation of multiaxial continuum damage mechanics for plain and fretting fatigue. Int J Fatig 2012;44(2): 260–72.
[35] Chen L, Chen Q, Shao E. Study on initiation and propagation angles of subsurface cracks in GCr15 bearing steel under rolling contact. Wear 1989;133(2):205–18.
[36] Harris TA, Barnsby RM. Life ratings for ball and roller bearings. ARCHIVE proceedings of the institution of mechanical engineers Part. J J Eng Tribol 1994-1996 (vols 208-210) 2001;215(6):577–95.
[37] Paulson NR, Sadeghi F, Habchi WA. Coupled finite element EHL and continuum damage mechanics model for rolling contact fatigue. Tribol Int 2016;107:173–83.
[38] Bomidi JAR, Sadeghi F. Three-dimensional finite element elastic–plastic model for subsurface initiated spalling in rolling contacts. J Tribol 2014;136(1), 011402. 1 [HYPHEN]14.